Progress In Electromagnetics Research, PIER 75, 253–269, 2007

OPTIMIZING THE COMPACT-FDTD ALGORITHM FOR ELECTRICALLY LARGE WAVEGUIDING STRUCTURES

M. F. Hadi and S. F. Mahmoud

Electrical Engineering
Kuwait University
P.O. Box 5969, Safat 13060, Kuwait

Abstract—This work investigates the unique numerical dispersion behavior of the Compact-FDTD method for waveguide analysis, especially when the waveguide dimensions are much larger than the operating wavelength as in high-frequency EMC analysis or radio-wave propagation in tunnels. The divergence of this dispersion behavior from the standard FDTD algorithm is quantified and a major source of dispersion error is isolated and effectively eliminated. Optimized modeling parameters in terms of appropriate spatial and temporal resolutions are generated for computationally efficient and error-free numerical simulations of electrically large waveguiding structures.

1. INTRODUCTION

The Compact-FDTD algorithm which was first proposed by Xiao, Vahldieck and Jin [1] as a borrowed technique from their work on the Transmission-Line-Method [2] allows full wave analysis of general waveguiding structures using a two-dimensional FDTD grid. In this algorithm the spatial derivative along the propagation direction (assumed along the z-axis in the present work) is evaluated analytically after restricting the entire EM fields' z-dependence to an $\exp[-\jmath\beta_z z]$ term, where $\jmath = \sqrt{-1}$. A careful substitution of this z-derivative will result in real-valued FDTD update equations—the format the algorithm settled with in its final incarnation [3, 4] for modeling lossless or weakly lossy waveguides. This idea of benefiting from analytically predictable modal field variations to compact the FDTD cell has been recently extended by Luo and Chen [5] to design one-dimensional FDTD modal absorbing boundary conditions for waveguide analysis where numerical simulation is executed along the waveguide axis and the field variations across the transverse plane are analytically imposed. Frequency domain versions of the Compact-FDTD algorithm have also appeared in the literature. Of special mention among them is the efficient, though mathematically intensive, multiresolution-based MRFD algorithm by Gokten, Elsherbeni and Arvas [6].

The advantages of the Compact-FDTD algorithm in terms of computing resources savings—though quite obvious—still fall short when the cross-sectional area of the waveguiding structure becomes large compared to the shortest wavelength of interest. Examples of such situations are high-frequency EMC analysis of microwave circuits and radiowave propagation in mine-shafts and railway tunnels [7, 8]. To illustrate the motivation of this work consider wave propagation through a lossless hollow metallic rectangular waveguide at a frequency high enough such that its cross-sectional dimensions are $4\lambda_o \times 2\lambda_o$. Fig. 1 shows this waveguide's dispersion curves for the first 8 TE_{m0}-only modes for simplicity. If the Compact-FDTD algorithm is used with the choice $\beta_z = 0.2\beta_o$, corresponding results will only correctly produce the group of modes just under the TE_{80} mode. To properly highlight the dominant TE_{10} mode behavior around the f_o operating frequency, the propagation constant must be chosen around $\beta_z = 0.99\beta_o$. Another class of waveguide applications where the propagation constant β_z approaches the unbounded wavenumber β includes metamaterial-inspired open dielectric waveguides which could support modes with $\beta_z = \beta$ as demonstrated by Lu, Wu and Kong [9]. As will be shown later in this work, such high β_z values present serious challenges to the Compact-FDTD algorithm in terms of excessive numerical dispersion errors.

In this work a condensed review of the Compact-FDTD algorithm will be presented, including the necessary modifications required to model lossy waveguides and anisotropic fill materials. Rigorous dispersion analysis will follow which will highlight the increasing modal solutions errors introduced as $\beta_z \to \beta_o$. The source of these increasing errors will be highlighted and a simple solution will be discussed and validated numerically through solutions of the dispersion relation and later through practical Compact-FDTD simulations.

2. REVIEW OF THE COMPACT-FDTD ALGORITHM

Replacing the z-derivative in Maxwell's equations with the $-\jmath\beta_z$ term will render the complex-valued time-domain equations

$$\epsilon\frac{\partial E_x}{\partial t} = \frac{\partial H_z}{\partial y} + \jmath\beta_z H_y \tag{1}$$

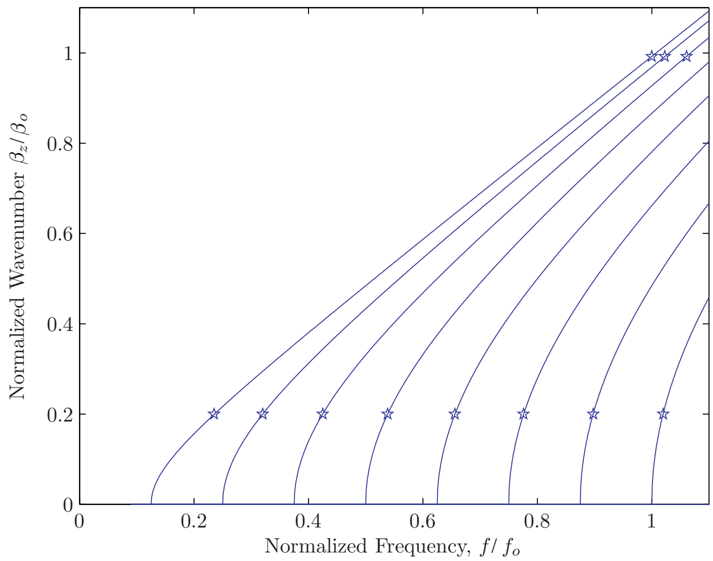

Figure 1. Effect of β_z choices on modal frequencies: Dispersion curves for a rectangular waveguide with dimensions $4\lambda \times 2\lambda$ at f_o. Only TE_{m0} modes are shown. The normalizing wavenumber is $\beta_o = 2\pi f_o/c$.

$$\epsilon \frac{\partial E_y}{\partial t} = -\frac{\partial H_z}{\partial x} - \jmath\beta_z H_x \tag{2}$$

$$\epsilon \frac{\partial E_z}{\partial t} = \frac{\partial H_y}{\partial x} - \frac{\partial H_x}{\partial y} \tag{3}$$

$$\mu \frac{\partial H_x}{\partial t} = -\frac{\partial E_z}{\partial y} - \jmath\beta_z E_y \tag{4}$$

$$\mu \frac{\partial H_y}{\partial t} = \frac{\partial E_z}{\partial x} + \jmath\beta_z E_x \tag{5}$$

$$\mu \frac{\partial H_z}{\partial t} = \frac{\partial E_x}{\partial y} - \frac{\partial E_y}{\partial x} \tag{6}$$

These equations when adapted directly by the FDTD method will produce complex-valued update equations. We should note however that the two field groups $\{E_x, E_y, H_z\}$ and $\{E_z, H_x, H_y\}$ will always be phase-shifted off each other by $\pi/2$. When the waveguide is composed of lossless or weakly lossy materials and when the fill dielectrics are isotropic, this phase shift could be prevented from producing complex update equations by replacing one of the two groups, say the first one, with $\{\jmath E_x, \jmath E_y, \jmath H_z\}$ [4] to produce[†]

$$\epsilon \frac{\partial E_x}{\partial t} = \frac{\partial H_z}{\partial y} + \beta_z H_y \tag{7}$$

$$\epsilon \frac{\partial E_y}{\partial t} = -\frac{\partial H_z}{\partial x} - \beta_z H_x \tag{8}$$

$$\epsilon \frac{\partial E_z}{\partial t} = \frac{\partial H_y}{\partial x} - \frac{\partial H_x}{\partial y} \tag{9}$$

$$\mu \frac{\partial H_x}{\partial t} = -\frac{\partial E_z}{\partial y} + \beta_z E_y \tag{10}$$

$$\mu \frac{\partial H_y}{\partial t} = \frac{\partial E_z}{\partial x} - \beta_z E_x \tag{11}$$

$$\mu \frac{\partial H_z}{\partial t} = \frac{\partial E_x}{\partial y} - \frac{\partial E_y}{\partial x} \tag{12}$$

Zhao, Juntunen and Raisanen [12] have demonstrated mathematically that expanding the complex-valued equations (1)–(6) will produce two decoupled and redundant sets of real-valued equations, one of which is represented by equations (7)–(12). They also verified that if the fill-dielectric is anisotropic, decoupling is still maintained as long as anisotropy is limited to one axis only. If dielectric anisotropy extends to more than one axis then decoupling is unattainable and the complex-valued equations need to be used for numerical simulations.

To accurately model loss-induced fast-attenuating waveguide modes, the z-derivative in Maxwell's equations must accommodate the attenuation factor as in $\exp[-(\alpha_z + \jmath\beta_z)z]$. This modification will result in a similar set of equations to (1)–(6), except that every $\jmath\beta_z$ occurrence is replaced with $\alpha_z + \jmath\beta_z$, and σE terms are injected in their usual places

$$\epsilon \frac{\partial E_x}{\partial t} = \frac{\partial H_z}{\partial y} + (\alpha_z + \jmath\beta_z) H_y - \sigma E_x \tag{13}$$

$$\epsilon \frac{\partial E_y}{\partial t} = -\frac{\partial H_z}{\partial x} - (\alpha_z + \jmath\beta_z) H_x - \sigma E_y \tag{14}$$

$$\epsilon \frac{\partial E_z}{\partial t} = \frac{\partial H_y}{\partial x} - \frac{\partial H_x}{\partial y} - \sigma E_z \tag{15}$$

$$\mu \frac{\partial H_x}{\partial t} = -\frac{\partial E_z}{\partial y} - (\alpha_z + \jmath\beta_z) E_y \tag{16}$$

[†] There seems to be some confusion in the literature regarding the re-mapped Maxwell's equations. The signs of the β_z terms are reversed in [4] for (8) and (10), and in [10] for (8) and (11). References [11] and [12] on the other hand contain the correct equations.

$$\mu \frac{\partial H_y}{\partial t} = \frac{\partial E_z}{\partial x} + (\alpha_z + \jmath\beta_z) E_x \tag{17}$$

$$\mu \frac{\partial H_z}{\partial t} = \frac{\partial E_x}{\partial y} - \frac{\partial E_y}{\partial x} \tag{18}$$

Wang, Shao and Wang [13] used these equations in an iterative technique that based input α_z choices on the decay (or growth) behavior of the simulated solutions with time. An overestimated α_z choice will cause solutions to decay while an underestimated choice will cause them to grow over time. Steady solutions over time on the other hand will signify an accurate α_z estimate.

For weakly lossy waveguides, α_z in (13)–(18) can be neglected and the resulting equations can be decoupled back to (7)–(12), with the added σE terms as in (13)–(15). The advantage being a reduction of simulation complexity and time at the expense of minimal errors as demonstrated later in the numerical experiments.

Fundamental to all Compact-FDTD variants is the z-compacted FDTD grid shown in Fig. 2 [3]. When second-order finite-differences are introduced, say, in equations (7)–(12) the Compact-FDTD update equations are produced, of which the following is an example

$$\begin{aligned} E_x|_{i,j}^{n+\frac{1}{2}} &= E_x|_{i,j}^{n-\frac{1}{2}} + \frac{\beta_z \Delta t}{\epsilon} H_y|_{i,j}^{n} \\ &\quad + \frac{\Delta t}{\epsilon \Delta y} \left(H_z|_{i,j+\frac{1}{2}}^{n} - H_z|_{i,j-\frac{1}{2}}^{n} \right) \end{aligned} \tag{19}$$

where Δt is the time step and Δy is the Compact-FDTD cell size along y. (In the remainder of this work $\Delta x = \Delta y = h$ will be assumed). A typical Compact-FDTD simulation would start by specifying a propagation constant β_z (and α_z when present) as an input with an appropriate initial field distribution that mimics the expected waveguide mode of interest.‡ The frequency response of the collected time series from the simulation will exhibit the guided modes pertaining to the chosen propagation constant. If $\beta_z = 0$ is chosen instead, the algorithm will produce the cutoff frequencies of the waveguide modes [2].

The dispersion relation and stability criterion for the Compact-FDTD algorithm were derived early in the literature by Cangellaris [14]

$$\left(\frac{h\sqrt{\mu\epsilon}}{\Delta t} \right)^2 \sin^2 \frac{\omega \Delta t}{2} = \sin^2 \frac{\tilde{\beta}_x h}{2} + \sin^2 \frac{\tilde{\beta}_y h}{2} + \left(\frac{\beta_z h}{2} \right)^2 \tag{20}$$

‡ Introducing a time function excitation here will simulate a line source extending along the axis of the waveguide which would complicate deriving the modal attenuation characteristics from the collected data.

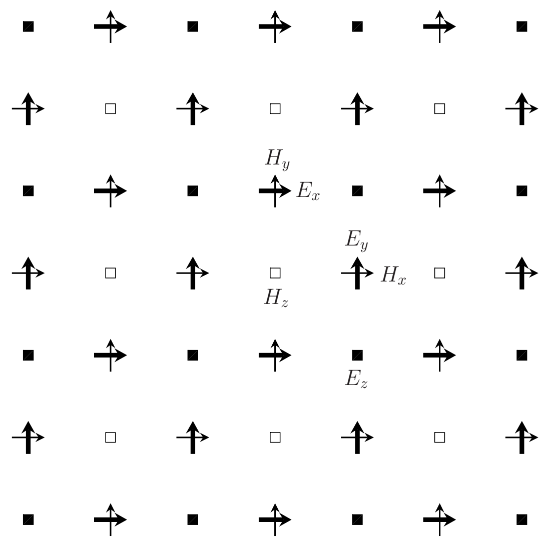

Figure 2. The Compact-FDTD grid. Bold and thin icons represent the E and H field nodes, respectively. Like-field components are equispaced by $\Delta x = \Delta y = h$.

$$\Delta t \le \frac{h\sqrt{\mu\epsilon}}{\sqrt{2 + \left(\frac{\beta_z h}{2}\right)^2}} \tag{21}$$

where $\sqrt{\tilde{\beta}_x^2 + \tilde{\beta}_y^2} = \tilde{\beta}_T$ is the numerically rendered transverse wavenumber by the Compact-FDTD algorithm.

3. NUMERICAL DISPERSION ANALYSIS

In his numerical dispersion analysis [14], Cangellaris used a rectangular hollow waveguide as an example and replaced $\tilde{\beta}_x$ and $\tilde{\beta}_y$ in the dispersion relation (20) with the theoretical $\beta_x = m\pi/a$ and $\beta_y = n\pi/b$ values, respectively, in an effort to predict the resonance frequencies and consequently the numerically rendered modal guide wavelengths. In reality, however, the main value of the FDTD dispersion relations in general is their accurate prediction of the *errors* in the numerically rendered wavenumbers. In the case of the Compact-FDTD algorithm for example, it is the $\tilde{\beta}_T$ deviation from $\beta_T = \sqrt{\beta_o^2 - \beta_z^2}$ that can be predicted by (20). The resonance frequencies on the other hand can only be produced from actual Compact-FDTD simulations.

In the following analysis the figure of merit of choice for numerical dispersion will be the Global Phase Error

$$\Phi = \frac{1}{2\pi}\int_0^{2\pi}\left|\tilde{\beta}_T - \beta_T\right|^2 d\phi \tag{22}$$

which is a square-error function averaged over all propagation angles ϕ within the Compact-FDTD grid. This error function will be evaluated and compared at several resolution factors among other variables. The resolution factor in the present context, however, requires some clarification. In normal, non-compact FDTD algorithms the resolution factor is conventionally defined as the number of FDTD cells per wavelength. Adopting such a definition for the Compact-FDTD algorithm is acceptable so long as the frequency range of interest is at the vicinity of the cutoff frequencies. When attempting to investigate modal solutions at higher frequencies with this resolution definition, the unbounded wavelength shrinks and the $h = \lambda/R$ values will become unnecessarily small and numerically costly.

The fact is, in modal analysis, the waveguide's transverse wavelength for any given mode is a function of the waveguide's dimensions and constituent parameters of its fill-materials and is independent of the frequency's proximity to the cutoff frequency; The entire H_z variation for the TE_{10} mode of a rectangular waveguide for example constitute a single half-cycle along the x-axis and no variation at all along the y-axis. Indeed, a single cell along the y-axis is all that is needed if only TE_{m0} modes are of interest. Given this fact, the Compact-FDTD grid discretization level should be referenced not to the unbounded wavelength λ but rather to the transverse wavelength $\lambda_T = 2\pi/\beta_T$ and β_T in turn is independent of frequency. More importantly, if one discretization level is good enough for one frequency to accurately analyze the mode's behavior then it is good enough for all higher operating frequencies for the same mode. This feature of the Compact-FDTD algorithm could allow simple and computationally efficient frequency dispersion analysis of elaborate waveguides in the Tera-Hertz [15] and optical [16] frequency ranges.

To generalize the discussion away from any specific waveguide example as befitting the general dispersion relation let us define $\beta_z = \kappa\beta$ where β is the unbounded wavelength and $\kappa \to 1$ as the frequency increases or equivalently, as the waveguide becomes electrically large. Using $\beta^2 = \beta_T^2 + \beta_z^2$ we can write

$$\lambda_T = \frac{2\pi}{\beta_T} = \frac{2\pi}{\sqrt{1-\kappa^2}\beta} = \frac{\lambda}{\sqrt{1-\kappa^2}} \tag{23}$$

and henceforth define the Compact-FDTD resolution factor as R cells per λ_T or $h = \lambda_T/R$.

Fig. 3 demonstrates the Global phase error deterioration as the normalized propagation constant κ approaches unity and the time step is kept at the maximum limit allowed by the stability criterion (21) for each κ value. This figure clearly shows that excessively high resolution factors are needed near the limiting value of $\kappa = 1$. The data in this figure and those in the following section were calculated assuming a 1 GHz operating frequency in an air-filled general waveguide ($\beta = 20.96\,\text{rad/m}$).

4. ALGORITHM OPTIMIZATION

Further analysis of the dispersion relation (and subsequent numerical simulations) have revealed that the time step Δt has a critical role to play in minimizing numerical dispersion errors. Whereas the maximum time step provides the least errors in the standard FDTD algorithm when modeling lossless media, for the compact-FDTD algorithm this is not the case as illustrated in Fig. 4. This figure demonstrates a rapid drop in error levels as the time step is reduced providing optimum choices for the courant number $\nu = \Delta t_{\max}/\Delta t$. The error levels reach optimum values at certain ν values that change with β_z choices. These optimum values invariably approach unity for all R values as $\kappa \to 0$ approaching at the limit the standard 2-D FDTD algorithm (See Table 1). Varying the dielectric constant produced identical data as in Fig. 4 and Table 1 which validates using the derived optimum ν values for inhomogeneously filled waveguides, provided that h and consequently $\Delta t_{\max}$ are based on the densest dielectric (or $\lambda_{T,\min}$) in the waveguide.

Table 1. Optimum Courant Numbers for the Compact-FDTD Algorithm, $\nu = \Delta t_{\max}/\Delta t$

$\kappa = \beta_z/\beta_o$	$R = 10$	$R = 20$	$R = 30$
0	1	1	1
0.80	2.2	2.2	2.3
0.90	3.9	4.2	4.2
0.95	6.9	7.9	8.2
0.97	10.3	12.6	13.2
0.99	22.2	32.3	36.4
0.995	33.7	54.8	65.7

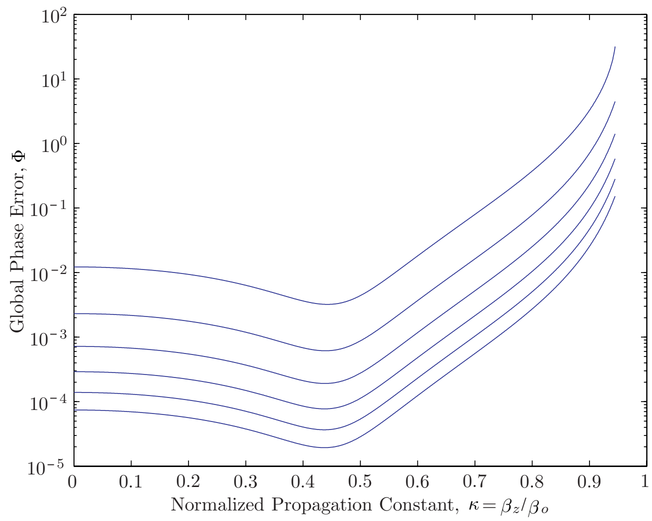

Figure 3. Effect of β_z choice on the Global Phase Error at the resolution factors (from top to bottom) $R = 10,\ 15,\ 20,\ 25,\ 30,\ 35$ cells per transverse wavelength at corresponding maximum allowable time steps. Operating frequency is 1 GHz or $\beta_o = 20.96\,\mathrm{rad/m}$.

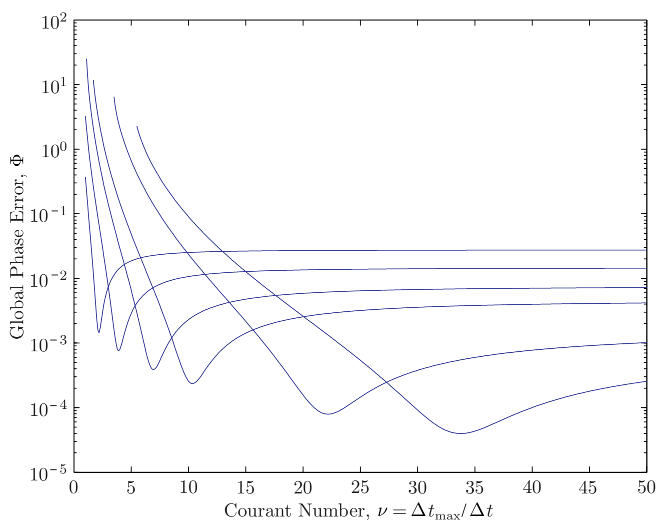

Figure 4. Sensitivity of the Global Phase Error to Δt choices. The six curves (from top to bottom at $\nu = 40$) correspond to $\beta_z/\beta_o = 0.8,\ 0.9,\ 0.95,\ 0.97,\ 0.99,\ 0.995$ with $R = 10$ at 1 GHz.

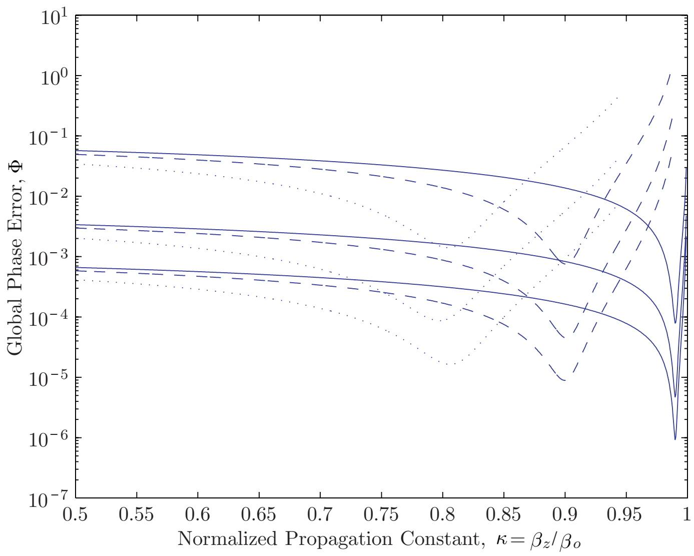

Figure 5. Sensitivity of the (β_z,Φ) dispersion curves to the time step choice (compare to Fig. 3). The three sets of curves were optimized for $\kappa = 0.8$ (dotted), 0.9 (dashed), and 0.99 (solid), and in each set the curves correspond (from top to bottom) to $R = 10,\ 20,\ 30$ cells per transverse wavelength λ_T.

To verify the time step optimization the numerical dispersion curves of Fig. 3 are recalculated using the optimum time steps and presented in Fig. 5, clearly demonstrating the advantage of time step optimization, especially as $\kappa \to 1$. For example, at $\kappa = 0.99$, the Global Phase Error has been reduced from near infinite value at $R = 10$ to roughly 10^{-4}.

An optimization that is based on reducing the time step independently from the spatial step has added advantages compared to reducing both in lock step as is usually done. If h is halved for example as a means of reducing numerical dispersion then the total simulation time steps required must be increased by at least $2^3 = 8$ times for the same total simulated time, $N\Delta t$, to accommodate the increased resolutions in all three pertinent axes, x, y and t. On the other hand halving Δt alone would only require doubling the number of time steps for the same total simulated time.

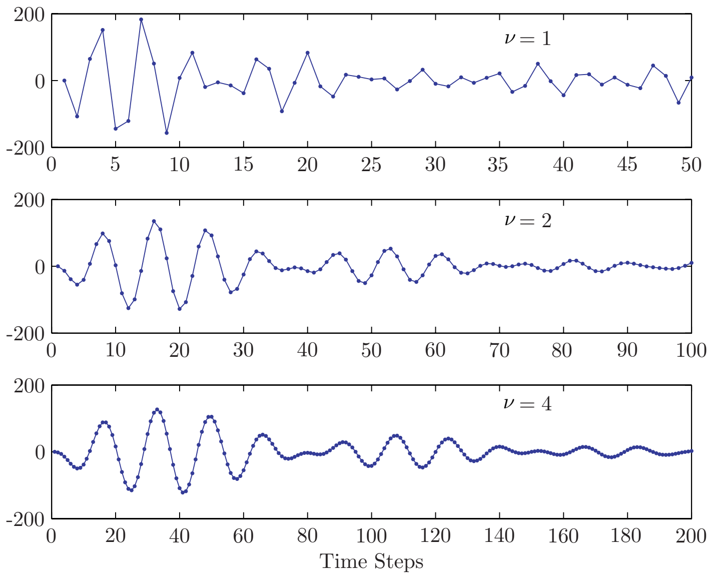

Figure 6. Effective temporal resolutions at different time step choices, demonstrating the Compact-FDTD's need for lower time steps (as $\kappa \to 1$) compared to the standard FDTD method. Plots are for the E_y field component.

5. NUMERICAL VALIDATION

A simple waveguide example is used here to validate the need for the proposed time step optimization. The waveguide has a rectangular cross section of $4\lambda \times 2\lambda$ at 1 GHz where it is assumed to operate; namely, $a = 1.199\,\mathrm{m}$ and $b = 0.5995\,\mathrm{m}$. The walls are assumed perfect conductors and the dielectric fill is homogeneous with $\epsilon_r = 1$ and σ is assumed finite to observe the effect of dielectric losses on solutions convergence. The waveguide cross-section is divided into a coarse 10×5 FDTD cells and β_z is chosen as $0.99\beta_o$ to closely observe the TE_{10} mode at the 1 GHz operating frequency. Initial field distribution is introduced for the H_z component with $H_z = -1$ for $x < a/2$ and $+1$ for $x > a/2$ which will excite the odd TE_{m0} modes.

Fig. 6 is presented to demonstrate first hand the need for moving away from the maximum time step as the condition $\kappa \approx 1$ generates an effective temporal resolution of under 4 steps per wave period at $\Delta t_{\max}$ even though spatial resolution is effectively 17.7 cells per λ_T (defined earlier) at 1 GHz. Fig. 7 tracks the convergence of TE_{10} resonance as the time step decreases for two dielectric loss choices

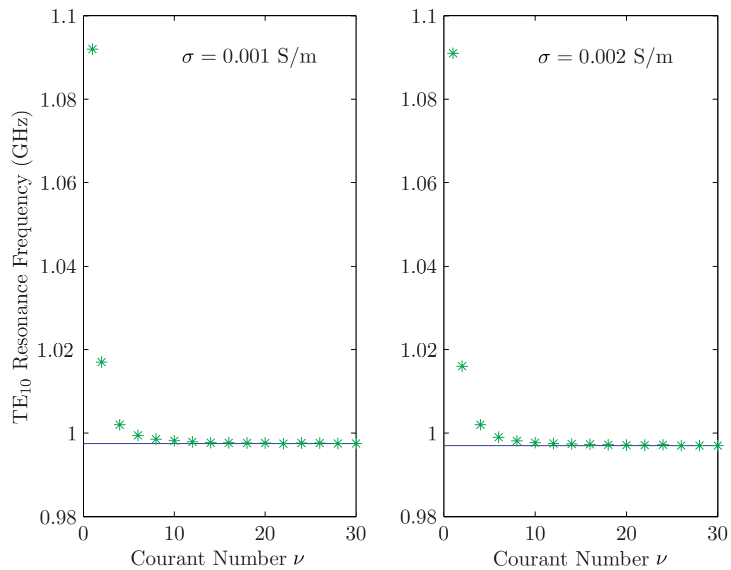

Figure 7. Homogeneously filled rectangular waveguide: Convergence of the TE_{10} mode resonance with time step reduction at two dielectric loss values. Good convergence is achieved at Courant numbers as small as $\nu = 10$.

($\sigma = 0.001,\ 0.002\,\mathrm{S/m}$). It is clear that resonance frequencies converge to their steady solutions with only a relatively moderate time step reduction, $\nu \approx 10$ or a time step that is one-tenth of the maximum allowable time step by the stability criterion.

Fig. 8 on the other hand which tracks the quality factor convergence, confirms the need for larger time step reductions ($\nu > 22$) to reach steady solutions. The attained quality factor values differ from the analytical values ($Q = \omega\epsilon/\sigma$ for homogeneously filled waveguides [17]) by 1.8% and 2.4% at $\sigma = 0.001,\ 0.002\,\mathrm{S/m}$, respectively. This is due to the coupling effect of the dielectric losses on the closely spaced resonance modes at the high 1 GHz operating frequency as demonstrated in the spectral power density plots of Fig. 9.

To investigate the effect of both waveguide inhomogeneity and losses the previous rectangular waveguide was allowed to be only partially filled as in ($\epsilon_r = 2, \sigma = 0.0005$) for $0 < x < a/2$ and ($\epsilon_o, \sigma = 0$) for $a/2 < x < a$. This is a well-known test problem of numerical techniques for waveguide structures [18, 19] and its theoretical analysis can be found in Harrington's classic EM book (Section 4.6) for the lossless case [20]. Again, it took a time step reduction of $\nu > 10$ to

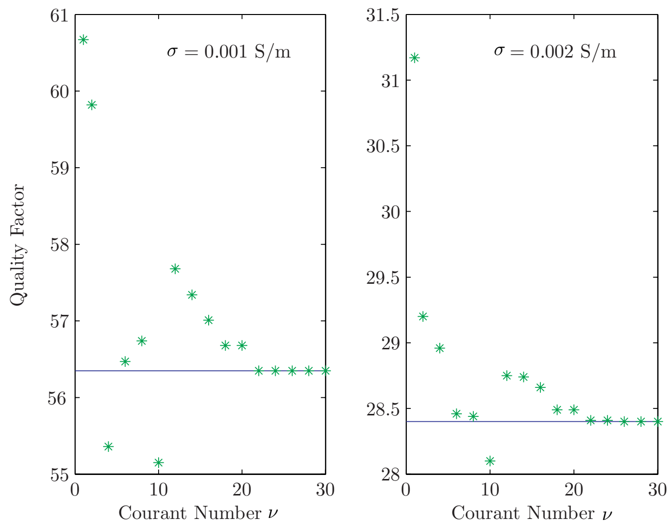

Figure 8. Homogeneously filled Rectangular Waveguide: Quality factor convergence requires twice as much time step reduction compared to resonance frequency convergence; $\nu > 22$.

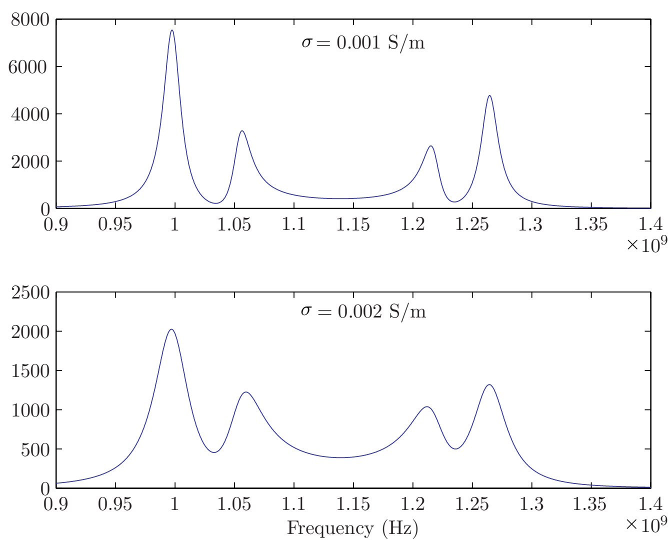

Figure 9. Power spectral density plots of the E_y field component in the homogeneously filled rectangular waveguide. Mode coupling increases with dielectric losses causing a slight deviation when graphically determining the quality factors.

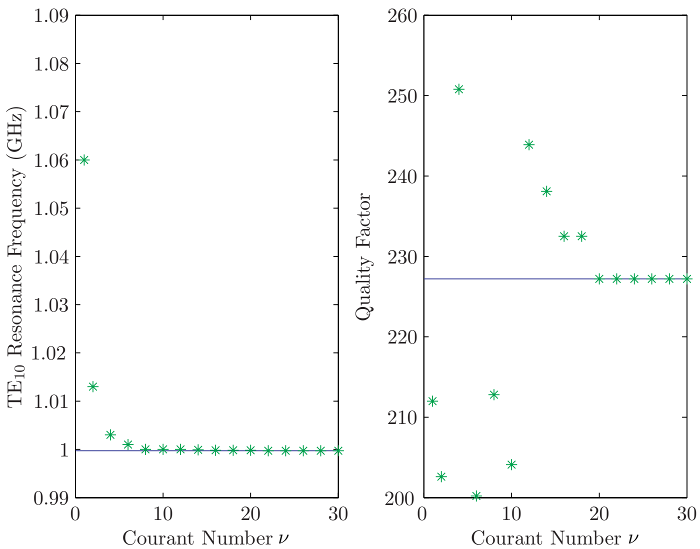

Figure 10. Convergence of the partially filled waveguide's TE_{10} mode resonance frequency and quality factor with time step reduction. To obtain the 1 GHz resonance frequency, β_z was chosen as $0.985\sqrt{\epsilon_r}\beta_o$.

obtain resonance frequency convergence for the TE_{10} mode and $\nu > 20$ to obtain quality factor convergence as summarized in Fig. 10. The converged quality factor value deviated from the analytical value by only 0.7% due to the reduced dielectric loss compared to the previous example, and consequently, reduced cross-modal coupling.

To appreciate the level of accuracy obtained in both examples of this section as well as the efficiency of the proposed optimization, it should be reiterated here that the spatial resolution used was only 10×5 FDTD cells for the entire cross-section of the electrically large $4\lambda_o\times2\lambda_o$ waveguide (at 1 GHz). Simulations were allowed to run for as high as 2^{21} time steps to achieve frequency resolutions high enough to collect data directly from the FFT plots. Even then run times were no longer than a couple of minutes each on an old portable PC. From the authors' previous experiences with Pade rational function approximation [21], post-FFT processing could have been used to drastically reduce FDTD run times while maintaining excellent articulation of closely spaced resonance frequencies. Conducted experiments, however, have shown that the quality factors in the above examples were unpredictably sensitive to the chosen Pade approximation model order.

6. CONCLUSION

When the frequency of interest is much higher than the modal cutoff frequencies of the investigated waveguide, the Compact-FDTD algorithm requires an input β_z value that is very close to the unbounded wavenumebr, β. This close proximity in turn causes a serious deviation of the numerical dispersion behavior of the Compact-FDTD algorithm from the well known behavior of the standard FDTD algorithm. This paper investigated in depth this unique dispersion behavior and demonstrated, in particular, the impossibility of getting any valid simulation results if the chosen time step is kept at or near the maximum value allowed by the stability criterion as favored by the standard FDTD algorithm.

Specific optimum Δt values were derived which allowed effective numerical dispersion reduction while keeping the spatial resolution coarse enough to track the modal distribution at the wavequide's cross-section. These optimum values are functions of the ratio β_z/β which approaches unity as the electrical size of the waveguide becomes large. They are however relatively insensitive to the spatial resolution except for extremely large waveguides which allows their general use in various cross-sectional geometries without the need for problem-specific optimization.

Numerical simulations were carried out that validated the positive effect of reducing the time step away from the maximum limits that include both inhomogeneities and dielectric losses within the waveguide's structure. Typical problems that could benefit from this algorithm optimization include EMC analysis of high-frequency signals coupling to waveguides and high frequency wave propagation in mine shafts and road and rail-way tunnels.

REFERENCES

1. Xiao, S., R. Vahldieck, and H. Jin, "Full-wave analysis of guided wave structures using a novel 2-D FDTD," *IEEE Microwave Guided Wave Lett.*, Vol. 2, No. 5, 165–167, May 1992.
2. Jin, H., R. Vahkdieck, and S. Xiao, "An improved TLM full-wave analysis using a two dimensional mesh," *IEEE MTT-S Int. Microwave Symp.*, 675–677, Boston, MA, June 1991.
3. Asi, A. and L. Shafai, "Dispersion analysis of anisotropic inhomogeneous waveguides using compact 2D-FDTD," *Electron. Lett.*, Vol. 28, No. 15, 1451–1452, July 1992.

4. Xiao, S. and R. Vahldieck, "An efficient 2-D FDTD algorithm using real variables," *IEEE Microwave Guided Wave Lett.*, Vol. 3, No. 5, 127–129, May 1993.
5. Luo, S. and Z. Chen, "An efficient modal FDTD for absorbing boundary conditions and incident wave generator in waveguide structures," *Progress In Electromagnetics Research*, PIER 68, 229–246, 2007.
6. Gokten, M., A. Z. Elsherbeni, and E. Arvas, "The multiresolution frequency domain method for general guided wave structures," *Progress In Electromagnetics Research*, PIER 69, 55–66, 2007.
7. Mahmoud, S. F., "Modal propagation of high frequency electromagnetic waves in straight and curved tunnels within the earth," *Journal of Electromagnetic Waves and Applications*, Vol. 19, No. 12, 1611–1627, 2005.
8. Pingenot, J., R. N. Rieben, D. A. White, and D. G. Dudley, "Full wave analysis of RF signal attenuation in a lossy rough surface cave using a high order time domain vector finite element method," *Journal of Electromagnetic Waves and Applications*, Vol. 20, No. 12, 1695–1705, 2006.
9. Lu, J., B.-I. Wu, and J. A. Kong, "Guided Modes with a linearly varying transverse field inside a left-handed dielectric slab," *Journal of Electromagnetic Waves and Applications*, Vol. 20, No. 5, 689–697, 2006.
10. Liu, F., J. E. Schutt-Ainé, and J. Chen, "Full-wave analysis and modelling of multiconductor transmission lines via 2-D-FDTD and signal-processing techniques," *IEEE Trans. Microwave Theory Tech.*, Vol. 50, No. 2, 570–577, Feb. 2002.
11. Pile, D. F. P., "Compact-2d fdtd for waveguides including materials with negative dielectric permittivity, magnetic permeability and refractive index," *Applied Physics B: Lasers and Optics*, Vol. 81, No. 5, 607–613, Sept. 2005.
12. Zhao, A. P., J. Juntunen, and A. V. Raisanen, "Relationship between the compact complex and real variable 2-D FDTD methods in arbitrary anisotropic dielectric waveguides," *IEEE MTT-S Int. Microwave Symp.*, Vol. 1, 83–87, Denver, CO, June 1997.
13. Wang, B.-Z., W. Shao, and Y. Wang, "2-d FDTD method for exact attenuation constant extraction of lossy transmission lines," *IEEE Microwave Wireless Compon. Lett.*, Vol. 14, No. 6, 289–291, June 2004.
14. Cangellaris, A. C., "Numerical stability and numerical dispersion of a compact 2D-FDTD method used for the dispersion analysis of

waveguides," *IEEE Microwave Guided Wave Lett.*, Vol. 3, No. 1, 3–5, Jan. 1993.

15. Zhang, J. and T. Y. Hsiang, "Dispersion characteristics of coplanar waveguides at subterahertz frequencies," *Journal of Electromagnetic Waves and Applications*, Vol. 20, No. 10, 1411–1417, 2006.
16. Maurya, S. N., V. Singh, B. Prasad, and S. P. Ojha, "Modal analysis and waveguide dispersion of an optical waveguide having a cross-section of the shape of a cardioid," *Journal of Electromagnetic Waves and Applications*, Vol. 20, No. 8, 1021–1035, 2006.
17. Johnk, C. T., *Engineering Electromagnetic Fields and Waves*, 2nd edition, John Wiley, New York, NY, 1988.
18. Zhou, X. and G. Pan, "Application of Physical Spline Finite Element Method (PSFEM) to fullwave analysis of waveguides," *Progress In Electromagnetics Research*, PIER 60, 19–41, 2006.
19. Xiao, J.-K. and Y. Li, "Analysis for transmission characteristics of similar rectangular guide filled with arbitrary-shaped inhomogeneous dielectric," *Journal of Electromagnetic Waves and Applications*, Vol. 20, No. 3, 331–340, 2006.
20. Harrington, R. F., *Time-Harmonic Electromagnetic Fields*, IEEE Press/Wiley-Interscience, New York, NY, 2001.
21. Hadi, M. F. and R. K. Dib, "Phase-matching the hybrid FV24/S22 FDTD algorithm," *Progress In Electromagnetics Research*, PIER 72, 307–323, 2007.